Steady dynamics of exothermic chemical wave fronts in van der Waals fluids

G. Dumazer,[1] C. Antoine,[1] A. Lemarchand,[1,*] and B. Nowakowski[1,2,3]

[1]*Laboratoire de Physique Théorique de la Matière Condensée, CNRS, Université Pierre et Marie Curie-Paris 6, UMR 7600, 4 Place Jussieu, Case Courier 121, 75252 Paris Cedex 05, France*

[2]*Polish Academy of Sciences, Institute of Physical Chemistry, 44/52 Kasprzaka, 01224 Warsaw, Poland*

[3]*SGGW, Physics Laboratory, Warsaw University of Life Sciences, Nowoursynowska 159, 02-776 Warsaw, Poland*

(Received 4 September 2009; revised manuscript received 21 October 2009; published 14 December 2009)

We study the steady dynamics of an exothermic Fisher-Kolmogorov-Petrovsky-Piskunov chemical wave front traveling in a one-dimensional van der Waals fluid. The propagating wave is initiated by a nonuniformity in reactant concentration contrary to usual combustion ignition processes. The heat release and activation energy of the reaction play the role of control parameters. We recently proved that the propagation of an exothermic chemical wave front in a perfect gas displays a forbidden interval of stationary wave front speeds [G. Dumazer, M. Leda, B. Nowakowski, and A. Lemarchand, Phys. Rev. E **78**, 016309 (2008)]. We examine how this result is modified for nonideal fluids and determine the effect of the van der Waals parameters and fluid density on the bifurcation between diffusion flames and Chapman-Jouguet detonation waves as heat release increases. Analytical predictions are confirmed by the numerical solution of the hydrodynamic equations including reaction kinetics.

DOI: 10.1103/PhysRevE.80.066309 PACS number(s): 47.70.Fw, 47.70.Pq, 82.40.Ck

I. INTRODUCTION

Reacting flows have a considerable wide range of applications, including combustion processes, plasma physics, phase transitions, chemical reactors, and biological signaling systems [1–7]. In particular, the propagation of exothermic chemical wave fronts in fluids is intensively studied [8–15]. Combustion waves such as premixed and diffusion flames or detonation waves are solutions of the hydrodynamic equations including chemical kinetics. The main nonlinearities of these equations are due to chemistry, since the reaction rates have a nonlinear dependence on temperature and species concentrations. The chemical mechanism often involves autocatalysis, known as chain-branching kinetics in hydrocarbon oxidation [4,16,17]. The simplest nonlinear chemical scheme is the quadratic reaction-diffusion model devised by Fisher and Kolmogorov-Petrovsky-Piskunov (F-KPP) in population dynamics [18,19]. The original F-KPP model has been extended to thermochemical systems [16,20] by introducing a heat Q as follows:

$$A + B \rightarrow 2A + \text{heat } Q. \tag{1}$$

In the thermoneutral case ($Q=0$), the density $\rho(x,t)$ is constant and the macroscopic evolution of the system is governed by a single reaction-diffusion equation for the concentration $\rho_A(x,t)$ of species A. This equation admits a family of wave front solutions, moving at constant speed U, and replacing the unstable $\rho_A=0$ stationary state by the stable $\rho_A=\rho$ stationary state. Steep enough initial profiles evolve to the marginally stable front propagating with the speed $U=2\sqrt{k\rho D}$, where k is the rate constant of the reaction (1) and D is the diffusion coefficient of species A and B [7]. For exothermic reactions ($Q>0$), chemistry is coupled to fluid dynamics, and the chemical concentration wave is accompanied by waves in all the flow-field variables (density, stream velocity, and temperature).

In this paper, we focus on the analysis of the steady dynamics of an exothermic chemical wave front propagating in a one-dimensional medium. We consider molecular conformational changes between species A and B [21] or autocatalytic isomerization [22–24], which are correctly modeled by the F-KPP scheme. These reactions involve relatively low values of the heat release and are fast, i.e., they are associated with small activation energy. As known in combustion, there exists several modes for which the wave front speed is controlled by totally different processes: mainly by reactive and diffusive processes for a diffusion flame and only by the heat release for a Chapman-Jouguet detonation wave [4,3,25]. The initiation process plays a key role in the ignition of a particular combustion mode. Ignition is generally triggered by a spatial nonuniformity—in parameters or variables—which creates the conditions for a spontaneous release of chemical energy and the development of a self-sustained exothermic wave. These spatial nonuniformities can be in dynamical variables (a pressure jump in a shock or a temperature jump in a "hot spot") or, less often, in species concentrations [26–28]. Here, we consider such an initial concentration jump where chemistry, and not hydrodynamics, initiates the combustion wave. We recently proved the existence of a forbidden interval of stationary wave front speeds for the F-KPP model in a perfect gas. We observed a bifurcation from a diffusion flame to a Chapman-Jouguet detonation wave when the activation energy is varied [14,29] and when the heat release Q is increased [15]. In the present paper, we extend this work to more realistic fluids such as a van der Waals fluid. Some features exhibited by reactive flows have already been studied in such real fluids [30–32]. Although not quantitatively exact, the van der Waals model has successfully given qualitative predictions of many properties exhibited by real fluids, such as dense gases and even liquids [33,34]. The two parameters of this model are the

*Corresponding author. FAX: +33(0)144277287. anle@lptmc.jussieu.fr

pressure and co-volume correction terms, a and b, which account for intermolecular attractive and repulsive forces, respectively. Here, we do not deal with anomalous fluid behaviors and choose the a and b parameters accordingly [30,35,36]. Our main goal is then to examine the effect of these correction terms on the steady dynamics of a combustion wave which is ignited by an initial discontinuity in a reactant concentration. In particular, we wish to examine the effect of fluid density on combustion wave dynamics. For illustration, we consider the reaction of isomerization of n-butene into isobutene on zeolithes for two different isobutene densities [22–24]. Isobutene is of fundamental interest for fuel combustion as an intermediate of the pyrolysis and oxidation of octane enhancers such as MTBE (methyl tert-butyl ether) and ETBE (ethyl tert-butyl ether). Combustion waves of isobutene have been essentially studied from the viewpoint of shock tube ignition experiments, in both laminar and turbulent regimes [37–39].

The paper is organized as follows. After briefly recalling the governing equations, we use the Rankine-Hugoniot jump conditions to derive the limits of the forbidden interval of stationary wave front speeds, first for a general equation of state and, then, for a van der Waals fluid. The analytical predictions are compared with the results of the numerical solutions of the hydrodynamic equations in the case of gaseous isobutene, for low and high fluid densities, and for different values of the activation energy and heat release of the reaction. Finally, we show how the bifurcation between different combustion modes is modified by the van der Waals parameters.

II. FORBIDDEN INTERVAL OF STATIONARY WAVE FRONT SPEEDS

We consider the one-dimensional evolution of a compressible viscous fluid. Its dynamics is governed by the following dissipative balance equations for total concentration $\rho(x,t)$ (mass continuity equation), stream velocity $u(x,t)$, internal energy density $e(x,t)$ and concentration $\rho_A(x,t)$ of species A:

$$\frac{d}{dt}\rho = -\rho\partial_x u, \tag{2}$$

$$\frac{d}{dt}u = -\frac{1}{m\rho}\partial_x(p-\sigma), \tag{3}$$

$$\frac{d}{dt}e = -\frac{p-\sigma}{\rho}\partial_x u - \frac{1}{\rho}\partial_x J_Q + \frac{RQ}{\rho}, \tag{4}$$

$$\frac{d}{dt}\rho_A = -\rho_A\partial_x u - \partial_x J_D + R, \tag{5}$$

where d/dt stands for the convective derivative $\partial_t + u\partial_x$, and where p, σ, J_Q, and J_D are the pressure, viscous stress tensor, heat flux, and diffusion flux, respectively. Q is the heat released by the exothermic process of the chemical mechanism of interest. The reaction rate R is a nonlinear function of $\rho_A(x,t)$. For example, $R=k\rho_A(\rho-\rho_A)$ for the F-KPP reaction given in Eq. (1), where k is the rate constant of the reaction.

When supplemented by linear constitutive relations, this nonlinear reactive hydrodynamic model is a system of partial differential equations which admits stable traveling wave solutions displaying a finite speed of propagation [6,30]. If the four variables ρ, ρ_A, u, and e have such a stationary wave front solution moving at speed U, then Eqs. (2)–(5) become:

$$0 = \partial_z(\rho v), \tag{6}$$

$$0 = \partial_z(m\rho v^2 + p - \sigma), \tag{7}$$

$$0 = \partial_z[m\rho v^3/2 + (p-\sigma)v + e\rho v + J_Q - Q(\rho_A v + J_D)], \tag{8}$$

$$R = \partial_z(\rho_A v + J_D), \tag{9}$$

with the comoving coordinates $z=x-Ut$ and $v=u-U$. Ahead and behind the front, the fluxes σ, J_Q, and J_D vanish since the flow-field variables ρ, ρ_A, u, and e (or p) are constant: ρ_1, ρ_{A_1}, v_1, e_1, and p_1 far ahead of the front and ρ_2, ρ_{A_2}, v_2, e_2, p_2 far behind it. The concentrations ρ_{A_1} and ρ_{A_2} are two steady states of the chemical reaction of interest (i.e., such that $R=0$): ρ_{A_2} is stable but ρ_{A_1} may be either stable (as for the Schlögl model [15,40] and Zeldovich-Frank-Kamenetskii Eq. [41].), or unstable [as for the F-KPP model (1) considered in this paper]. The Rankine-Hugoniot jump conditions [3,4,25] are deduced from Eqs. (6)–(8):

$$\rho_2 v_2 = \rho_1 v_1, \tag{10}$$

$$p_2 + m\rho_2 v_2^2 = p_1 + m\rho_1 v_1^2, \tag{11}$$

$$e_2 + \frac{p_2}{\rho_2} + m\frac{v_2^2}{2} - Q\frac{\rho_{A_2}}{\rho_2} = e_1 + \frac{p_1}{\rho_1} + m\frac{v_1^2}{2} - Q\frac{\rho_{A_1}}{\rho_1}. \tag{12}$$

Let us stress again that they do not depend on the hydrodynamic fluxes and transport coefficients.

Substituting ρ_2 from Eq. (10) and p_2 from Eq. (11) in Eq. (12), one obtains a relation between ρ_{A_2}, v_2, and e_2 and ρ_1, ρ_{A_1}, v_1, e_1, and p_1. When supplemented by the equation of state of the fluid $p(\rho,T)$ and its caloric equation of state $e(\rho,T)$, where T is the temperature, this relation reads:

$$f(v_2,v_1,\rho_1,T_1,\rho_{A_1},\rho_{A_2},Q) = 0, \tag{13}$$

where the function f is often a polynomial in the variable v_2 or, equivalently, in $v_2/v_1=X$. The condition that Eq. (13) must have real roots gives constraints on v_1, ρ_1, T_1, ρ_{A_1}, ρ_{A_2}, and Q which imply forbidden intervals of $v_1=u_1-U$, i.e., of U when $u_1=0$ (unperturbed steady state ahead of the front, as in the F-KPP model). Only nonstationary wave fronts can exist if U belongs to this "forbidden" domain $\overline{\mathcal{D}_U}$, the limits of which are denoted by $U_i(\rho_1,T_1,\rho_{A_1},\rho_{A_2},Q)$. For instance, the perfect gas case with $\rho_{A_1}=0$ and $\rho_{A_2}=\rho_2$ (as in the F-KPP model) leads to a unique forbidden interval $\overline{\mathcal{D}_U}=(U_{PG-},U_{PG+})$ delimited by the two branches obtained as the heat release Q varies [14,15]:

$$U_{PG\pm} = \sqrt{\frac{15k_BT_1 + 16Q \pm 4\sqrt{2Q(15k_BT_1 + 8Q)}}{9m}}, \tag{14}$$

where k_B is the Boltzmann constant. Our aim is to investigate to what extent the expression of the two branches are modified by the introduction of a different equation of state.

We consider the following generic equation of state (EOS):

$$p(\rho,T) = k_BT\rho g(\eta) - a\rho^2, \tag{15}$$

which is particularly well suited to model the short-range repulsion and long-range attraction of a hard-sphere fluid [34]. Here $\eta = \pi\rho d^3/6$ is the usual packing fraction (reduced density) which accounts for the excluded volume per sphere of diameter d, and the term $-a\rho^2$ is related to an attractive long-range interparticle potential which is added as a correction to the hard-sphere interaction. Different expressions of $g(\eta)$ have been devised so far. For example, for the perfect gas model, one has $g(\eta)=1$ and $a=0$, and one recovers the van der Waals EOS for $g(\eta)=1/(1-4\eta)$ where the term $4\eta/\rho=b$ stands for the van der Waals co-volume parameter. A more accurate model is given by the semiempirical Carnahan-Starling EOS [34,42,43] for which $g(\eta)=(1+\eta+\eta^2+\eta^3)/(1-\eta)^3$. The latter has been shown to be in excellent agreement with molecular dynamics simulations over the entire fluid range [34]. For low values of η, however, the van der Waals and Carnahan-Starling EOS give close results. Whatever the exact expression of $g(\eta)$, the caloric EOS for the internal energy density e is given by:

$$e(\rho,T) = \frac{3}{2}k_BT - a\rho, \tag{16}$$

provided $g(\eta)$ and a do not depend on T. With Eqs. (15) and (16), Eq. (13) for the F-KPP model ($\rho_{A_1}=0$ and $\rho_{A_2}=\rho_2$) becomes:

$$\frac{3}{g(B/4X)}\left(X(1+G) - GX^2 + \frac{A}{X}\right) - \left(2 + G + 2H - 2X(1+G) + GX^2 - 2A + 2\frac{A}{X} + \frac{3}{g(B/4)}(1+A)\right) = 0, \tag{17}$$

where $X=v_2/v_1$ and:

$$A = \frac{a\rho_1}{p_1/\rho_1} = \frac{a\rho_1}{k_BT_1}\frac{1}{g(B/4) - a\rho_1/k_BT_1}, \tag{18}$$

$$B = b\rho_1 = 4\eta_1, \tag{19}$$

$$G = \frac{mv_1^2}{p_1/\rho_1} = \frac{mv_1^2}{k_BT_1}\frac{1+A}{g(B/4)}, \tag{20}$$

$$H = \frac{Q}{p_1/\rho_1} = \frac{Q}{k_BT_1}\frac{1+A}{g(B/4)}. \tag{21}$$

If $g(\eta)$ is a polynomial fraction, Eq. (17) leads to a polynomial equation in X. The higher its degree, the higher the number of constraints on A, B, G, and H for the roots of Eq. (17) to be real. Eventually, the (Q,U) plane is split into several domains, each one corresponding to a different number of real roots of Eq. (17). The domain which is forbidden to stationary wave fronts, $\mathcal{D}_U$, is the one with no real roots.

Two different functions $g(\eta)$ for two different EOS may lead to different forbidden domains. As a result, a chemical wave front can be stationary for a particular EOS but not for another one. This effect can be easily understood by considering the forbidden domain $\mathcal{D}_U$ in the limit of vanishing heat release. For $Q\to 0$, indeed, $\mathcal{D}_U$ often reduces to a single velocity: the isentropic speed of sound U_S. This speed is strongly model dependent and is given by the formula [25]:

$$U_S^2 = \left(\frac{\partial p}{\partial \rho}\right)_S = \left(\frac{\partial p}{\partial \rho}\right)_T + \frac{T}{C_V\rho^2}\left(\frac{\partial p}{\partial T}\right)_\rho^2, \tag{22}$$

where $C_V=(\partial e/\partial T)_V$ is the molar heat capacity at constant volume of the fluid of interest. For the equations of state given in Eqs. (15) and (16), one obtains the same expression $C_V=\frac{3}{2}k_B$ as for the perfect gas. The sound speed then becomes:

$$U_S^2 = -2a\rho_1 + k_BT_1\left[g(\eta_1) + \eta_1 g'(\eta_1) + \frac{2}{3}(g(\eta_1))^2\right], \tag{23}$$

from which one recovers the expressions:

$$U_{S_{PG}}^2 = \frac{5}{3}k_BT_1 \tag{24}$$

$$U_{S_{vdW}}^2 = k_BT_1\left(\frac{5}{3(1-b\rho_1)^2} - 2\frac{a\rho_1}{k_BT_1}\right) \tag{25}$$

$$U_{S_{CS}}^2 = k_BT_1\left(\frac{5 + 10\eta_1 - 3\eta_1^2 + 8\eta_1^3 - 9\eta_1^4 + 22\eta_1^5 - \eta_1^6}{3(1-\eta_1)^6} - 2\frac{a\rho_1}{k_BT_1}\right) \tag{26}$$

for the perfect gas, van der Waals and Carnahan-Starling EOS, respectively. Figure 1 gives isotherms in the $\left(\frac{U_{S_{vdW}}}{U_{S_{PG}}}, \frac{\rho}{\rho_c}\right)$ plane where $\rho_c=1/(3b)$ is the critical density of a van der Waals fluid. For the chosen values of a and b, $U_{S_{vdW}}$ is smaller than $U_{S_{PG}}$ for a subcritical gas and is larger than $U_{S_{PG}}$ for a liquid and a supercritical fluid at sufficiently large temperature and density. It is clear from Eq. (25) that $U_{S_{vdW}}$ can be higher or lower than $U_{S_{PG}}$ according to the values of a and b [32,35]. In particular, the effect of parameter a is to lower the speed of sound in the fluid. Similarly, one can easily show that both $U_{S_{vdW}}$ and $U_{S_{CS}}$ increase with $b\rho_1(=4\eta_1)$. As a result, the forbidden domains associated with these different EOS do not have the same behavior as $Q\to 0$. For high values of Q, however, the Q dependence prevails over the a and b influence, mitigating the differences due to different EOS. In the following, we illustrate these effects with the van der Waals EOS.

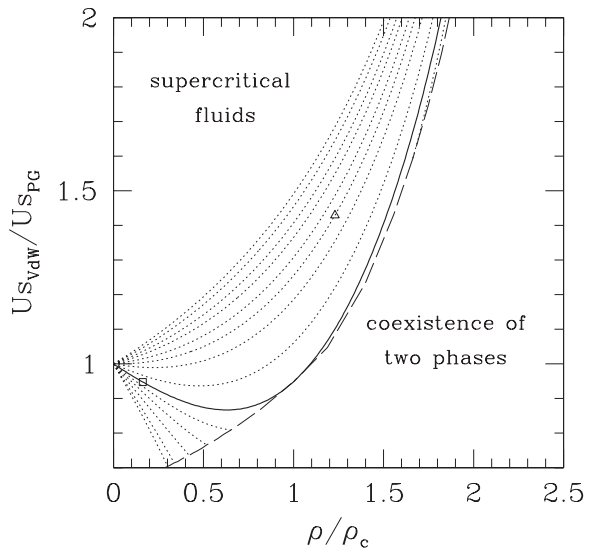

FIG. 1. Scaled van der Waals sound speed $U_{S_{vdW}}/U_{S_{PG}}$ isotherms (dotted lines), where $U_{S_{PG}}$ is the perfect gas sound speed versus scaled density ρ/ρ_c. The solid line corresponds to the critical temperature T_c. The dashed line is the saturation curve at which the gas and liquid phases coexist. The square and the triangle give the sound speed values in gaseous critical isobutene ($\rho/\rho_c=0.163$ and $T=T_c$) and in dense, supercritical isobutene ($\rho/\rho_c=1.23$ and $T=2T_c$), respectively.

III. APPLICATION TO VAN DER WAALS FLUIDS

The van der Waals EOS is the most natural extension of the perfect gas EOS. It reads:

$$p(\rho,T)=\frac{k_BT\rho}{1-b\rho}-a\rho^2, \tag{27}$$

where the pressure and volume correction terms a and b account, respectively, for the smooth, long-range, intermolecular attractive forces and the harsh, short-range, intermolecular repulsive forces or, equivalently, the finite molecular size. Most of intermolecular pair potentials, including the Lennard-Jones and hard-sphere potentials, can be split into such repulsive and attractive parts. This explains why, despite its shortcomings, the van der Waals model provides a clear physical picture of fluids and gives simple, but non trivial, semiquantitative explanations of deviations from the perfect gas model [33,34].

For the van der Waals EOS, Eq. (17) leads to a fourth-order polynomial equation in $X=v_2/v_1$:

$$4GX^4-(5+5G+3BG)X^3+[5+2H+G(1+3B)+A(1-3B)]X^2-AX+3AB=0. \tag{28}$$

From Sturm's theorem, it is then straightforward to show that there may be 0, 2, or 4 distinct, (positive) real roots. Therefore, there may be two distinct constraints on A,B,G,H parameters, splitting the (Q,U) plane into three distinct domains with either 0 (forbidden domain), 2, or 4 real solutions. For realistic values of A and B (for gases and supercritical fluids) however, only one constraint and two domains are present, as for the perfect gas. The constraint is then obtained when these two roots switch from real to complex, that is, when they coincide. An explicit expression of this constraint $G(A,B,H)$ can be obtained through the analytical expression of the roots of Eq. (28) [44]. However, we rather focus on the expansion of $G(A,B,H)$ to the first order in $A=a\rho_1^2/p_1$, since it gives a good approximation of the constraint even for large values of A and enables us to clearly see the deviations from the perfect gas model.

Equating the two real roots of Eq. (28) yields the following implicit condition on G to the first order in A:

$$h_1(G)+Ah_2(G)+O(A^2)=0, \tag{29}$$

with:

$$h_1(G)=[16G(5+G+3BG+2H)-(5+5G+3BG)^2]/G^2, \tag{30}$$

$$h_2(G)=\left[16G(1-3B)-8G\left(\frac{5+5G+27BG}{5+G+3BG+2H}\right)+24BG\left(\frac{5+5G+3BG}{5+G+3BG+2H}\right)^2\right]/G^2. \tag{31}$$

By expanding G in small A, we eventually find the expression of the two branches delimiting the forbidden domain $\overline{\mathcal{D}_U}$:

$$\frac{m}{k_BT_1}U_{vdW\pm}^2=\frac{1}{(1-B)(1+A)}\left[G_{0\pm}-A\frac{h_2(G_{0\pm})}{h_1'(G_{0\pm})}+O(A^2)\right], \tag{32}$$

where $G_{0\pm}$ are the two roots of the equation $h_1(G)=0$:

$$G_{0\pm}=\frac{15(1-B)+16H\pm4\sqrt{30(1-B)H+16H^2}}{9(1-B)^2}. \tag{33}$$

From the prefactor $1/(1-B)(1+A)$ in Eq. (32), one can infer the global changes due to A and B compared to the perfect gas model: B mainly shifts the domain $\overline{\mathcal{D}_U}$ upward without altering its shape, whereas A shifts $\overline{\mathcal{D}_U}$ downward. The zeroth order terms $G_{0\pm}$ do not alter these overall effects. The first-order term in brackets in Eq. (32), $-Ah_2(G_{0\pm})/h_1'(G_{0\pm})$, mainly changes the distance between the two branches of $\overline{\mathcal{D}_U}$, moving them apart or bringing them closer according to the values of H and B. For small heat release ($H\ll1$), the two branches move away if $B>1-\sqrt{20/27}\simeq0.139$ and get closer if not, this change being hard to detect since the two branches merge into a single speed—the speed of sound $U_{S_{vdW}}$ (Eq. (25))—in the limit $H\to0$. For high values of H, on the contrary, the change in the distance between the two branches can be clearly discriminated. The condition for they move away is now $B>2(\sqrt{41/36}-1)\simeq0.134$.

IV. NUMERICAL RESULTS AND DISCUSSION

A. Resolution of the balance equations for two van der Waals fluids

We solve the hydrodynamic equations for isobutene whose selective preparation on appropriate pore size zeolites

is known to be achieved through a bimolecular mechanism of F-KPP type [22–24]. Isobutene is used in the production of rubber for the tire industry and in manufacturing processes for plastics, antioxidants, and fine chemicals. Additionally, isobutene is the source material of polyisobutene, which is a precursor material for adhesives and sealants as well as lubricant and fuel additives, in particular the antiknock agents MTBE and ETBE.

The results of Sec. III are applied to isobutene of mass $m=9.3\times10^{-26}$ kg. Using the expression of the van der Waals constants, $a=\frac{27(k_BT_c)^2}{64p_c}$ and $b=\frac{k_BT_c}{8p_c}$, as functions of the critical temperature $T_c=418.3$ K and the critical pressure $p_c=40.01\times10^5$ Pa of isobutene, we obtain: $a=1.274$ Pa m^6 mol^{-2} and $b=1.086\times10^{-4}$ m^3 mol^{-1}. These values impose the critical density $\rho_c=1/(3b)$ and the molecular diameter $d=(\frac{3b}{2\pi})^{1/3}$ [45].

The balance equations [Eqs. (2)–(5)] are written for the following expressions of the viscous stress tensor, $\sigma=(4\eta/3+\zeta)\partial_x u$ with shear viscosity $\eta=\frac{5}{16d^2}\sqrt{\frac{mk_BT}{\pi}}$ and bulk viscosity $\zeta=\frac{b\rho^2}{\pi d^2}\sqrt{\frac{mk_BT}{\pi}}$, heat flux $J_Q=\lambda\partial_x T$ with thermal conductivity $\lambda=\frac{75k_B}{64d^2}\sqrt{\frac{k_BT}{\pi m}}$, diffusion flux $J_D=D\rho\partial_x(\rho_A/\rho)$ with diffusion coefficient $D=\frac{3}{8d^2\rho}\sqrt{\frac{k_BT}{\pi m}}$, reaction rate $R=k\rho_A(\rho-\rho_A)$ with rate constant obeying $k=4d^2\sqrt{\frac{\pi k_BT}{m}}\exp(-\frac{E_a}{k_BT})$, where E_a is the activation energy. The system is initially homogeneous except from the chemical point of view: we start from a step function for the concentration of species A with $\rho_A=\rho_0$ for $x\leq0$ and $\rho_A=0$ for $x>0$. As mentioned in the introduction, there is no initial hydrodynamic discontinuity contrary to usual combustion processes. In order to illustrate the different typical behaviors predicted by the analytical study, the stationary propagation speed of the reactive interface is computed numerically for different heat releases Q in the range $10^{-4}\leq Q/(k_BT_0)\leq1$ and different activation energies E_a in the range $1\leq E_a/(k_BT_0)\leq1.87$.

We use the Euler method to solve Eqs. (2)–(5). Space and time are discretized. The spatial cell length Δx is chosen such that the width of the reactive interface, $w=8\sqrt{D/(k\rho)}$, is equal to 65 cells for $Q=0$, i.e., for constant ρ and T since the hydrodynamic variables are no more coupled to the chemical reaction in this case. A too steep reactive interface could lead to numerical instabilities and a too large one would result in a useless increase in the integration time: a width of 65 cells offers a good compromise. Due to the propagation of the reactive interface, we must increase the length L of the medium during the computation. At each time step, we check the values of the hydrodynamic variables ρ, u, and T in cells 50 and $L/\Delta x-50$. As soon as the value of one of these variables differs (at the computing precision) from its initial value, we extend the system by one cell at the corresponding boundary. Hence, we keep an unperturbed boundary layer of 50 cells at each extremity of the one-dimensional medium during the whole simulation. The time step Δt is chosen such that the speed of the reactive interface, $U=2\sqrt{k\rho D}$, remains of the order of 0.01 cells per time step for $Q=0$ whatever the value of the activation energy. More precisely, we impose $U\Delta t/\Delta x=0.01\sqrt{6}\exp(-E_a/k_BT_0)$, which ensures that the reactive interface advances less than one cell per time step for all the considered values of the activation energy.

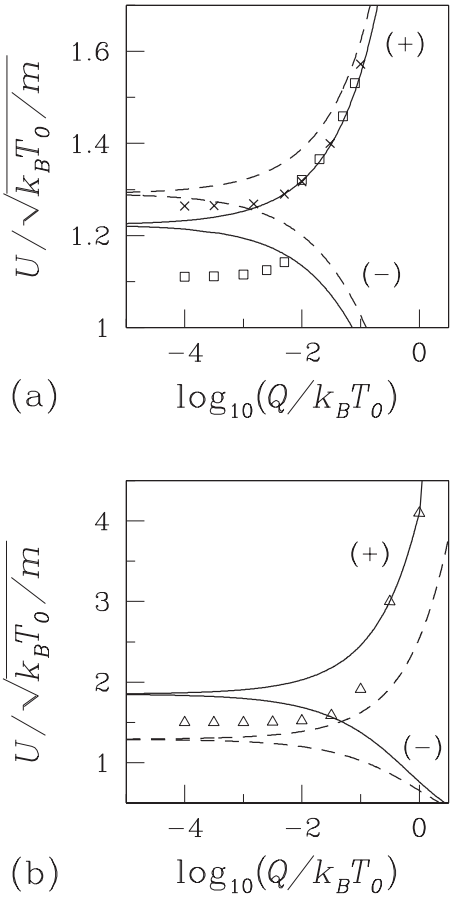

FIG. 2. Scaled speed $U/\sqrt{k_BT_0/m}$ of the reactive interface versus scaled heat release $Q/(k_BT_0)$ in logarithmic scale for (a) critical isobutene initially at ($\rho_0=0.163\rho_c$, $T_0=T_c$) for $E_a/k_BT_0=1.34$ (crosses) and $E_a/k_BT_0=1.6$ (squares), and (b) dense, supercritical isobutene initially at ($\rho_0=1.23\rho_c$, $T_0=2T_c$) for $E_a/k_BT_0=1$ (triangles). Dashed lines give upper (+) and lower (−) branches, U_{PG+} and U_{PG-}, respectively, of the forbidden domain for a perfect gas. Solid lines give upper (+) and lower (−) branches, U_{vdW+} and U_{vdW-}, respectively, of the forbidden domain for a van der Waals fluid.

We consider two typical van der Waals fluids. The case of a critical gas is illustrated with gaseous isobutene at density $\rho_0=0.163\rho_c$, initially at rest ($u_0=0$), and at temperature $T_0=T_c$. The reactive interface width and speed conditions impose ($\Delta x=0.72$ nm, $\Delta t=28.9$ fs) and ($\Delta x=0.82$ nm, $\Delta t=32.9$ fs) for the activation energy values $E_a=1.34k_BT_0$ and $E_a=1.6k_BT_0$, respectively. We give in Fig. 2(a) the two series of results for these two activation energies. The case of a dense fluid is illustrated by supercritical isobutene at density $\rho_0=1.23\rho_c$, initially at rest ($u_0=0$), and at temperature $T_0=2T_c$. For $E_a=k_BT_0$, we find ($\Delta x=0.08$ nm, $\Delta t=3.21$ fs). The stationary speeds of the reactive interface deduced from the numerical integration of the balance equations for the dense, supercritical fluid are given in Fig. 2(b).

Similarly to what was reported in references [14,15] for a perfect gas, three typical situations are observed for a van der Waals fluid: depending on the activation energy and the heat release, the reactive interface may be a supersonic diffusion

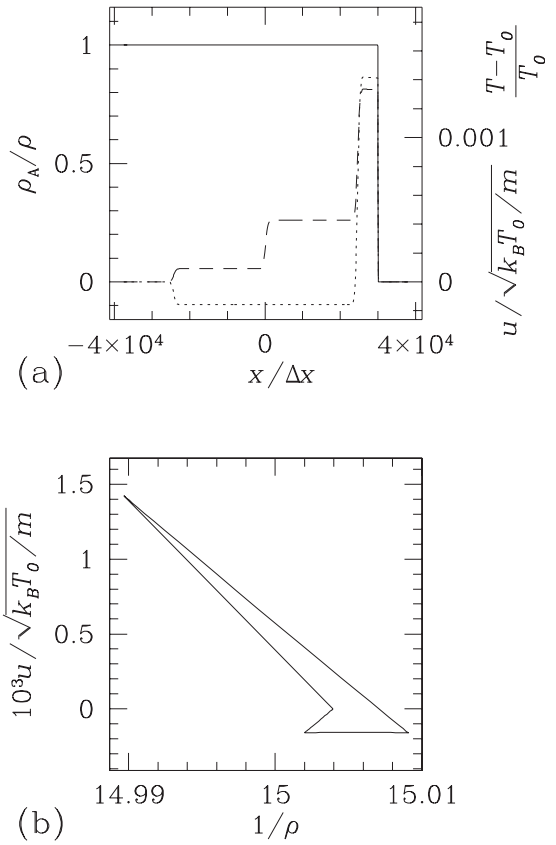

FIG. 3. Numerical solution of the reactive hydrodynamic equations [Eqs. (2)–(5)] for critical isobutene initially at ($\rho_0=0.163\rho_c$, $T_0=T_c$) for an activation energy $E_a=k_BT_0$ and a heat release $Q=10^{-3}k_BT_0$ after 2×10^6 integration time steps. (a) Left axis: scaled concentration profile ρ_A/ρ of species A (solid line). Right axis: scaled temperature shift $(T-T_0)/T_0$ (dashed line) and scaled stream velocity $u/\sqrt{k_BT_0/m}$ (dotted line). (b) Scaled stream velocity $10^3u/\sqrt{k_BT_0/m}$ vs reciprocal of density $1/\rho$.

flame, a subsonic diffusion flame, or a Chapman-Jouguet detonation wave.

B. Supersonic diffusion flame

For sufficiently small values of activation energy E_a and heat release Q, the speed of the reactive interface is higher than the sound speed. This first case is illustrated in Fig. 3(a) where the reactive interface (the step for ρ_A/ρ) is the first one from the right. Such a supersonic chemical front is known as a fast diffusion flame in the domain of combustion and corresponds to the weak detonation part of the Hugoniot-Crussard curve [3,4,25,46] although it does not have a detonation structure. It is to be noted that such supersonic diffusion flames are obtained in the case of the F-KPP model for extremely fast chemical reactions, that are associated with activation energies of the order of k_BT_0. This situation cannot be observed in the case of the Schlögl model, for which the speed of the diffusion flame remains smaller than the sound speed, even in the limit of a vanishing activation energy [15]. In Fig. 3(a), the step in the temperature profile, close to $x=0$, is reminiscent of the initial condition: At time $t=0$, species A and B come into contact, the autocatalytic reaction $A+B\rightarrow 2A$ is initiated and heat begins to be released in the two opposite directions. This step is known as a contact or degenerate tangential discontinuity and is associated with a step for density and temperature only, the pressure and stream velocity remaining constant across the discontinuity [25]. The exothermicity of the reaction at the interface between particles A and B generates two heat fronts or shock waves that propagates to the left and to the right. The second and fourth steps from the right in the temperature and stream velocity profiles are the shock waves which propagate in front of and behind the reactive interface. Following the first Rankine-Hugoniot jump condition given in Eq. (9), we have $u=-\rho_0U/\rho+U$ for stationary fronts traveling at speed U. According to Fig. 3(b), the four straight lines in the $(u,1/\rho)$ diagram are associated with the four stationary interfaces of speed given by the y intercept. In the case of a supersonic chemical front, the reactive interface propagates toward a nearly unperturbed medium at a temperature very close to T_0. Since the propagation speed of the F-KPP front is determined by the leading edge [6,7,47], the chemical front propagates at a speed very close to the thermoneutral speed $U(Q=0)=2\sqrt{k(T_0)\rho_0D(\rho_0,T_0)}$. Consequently, the speed of the reactive interface is nearly independent of Q in the case of a supersonic chemical front.

C. Subsonic diffusion flame

For sufficiently high activation energies and still sufficiently small heat releases, a second case is observed, for which the speed of the reactive interface is smaller than the sound speed. Then, the shock wave is propagating in front of the reactive interface, as shown in Fig. 4. In such a case of a subsonic chemical front (weak deflagration), the speed of the F-KPP reactive interface slightly increases with Q, since the medium in front of the reactive interface is perturbed and heated by the shock wave.

D. Chapman-Jouguet detonation wave

Finally, for sufficiently high values of the heat release Q, and whatever the activation energy E_a, the speed of the reactive interface is given by the upper branch $U_{vdW+}(Q)$ of the forbidden domain, as observed in Fig. 2. In this third case, only three stationary interfaces are observed, as shown in Fig. 5(a). In addition, a continuously stretching interface known as a self-similar rarefaction wave is observed behind the reactive interface [25]. The nonstationary character of the stretching interface is revealed by the curved upper line in the $(u,1/\rho)$ diagram in Fig. 5(b). The selection of the marginally stable speed on the branch U_{vdW+} is an illustration of the Chapman-Jouguet criterion [3,4,25,46], introduced for describing supersonic, detonative combustion modes that are ignited by a pressure or temperature jump and self-sustained by the heat release. The Chapman-Jouguet regime corresponds to the slowest possible detonation wave.

E. Bifurcation between a diffusion flame and a Chapman-Jouguet detonation wave

In our case, as heat release is increased, a bifurcation is observed for a critical value Q_c. For $Q<Q_c$, the speed of the

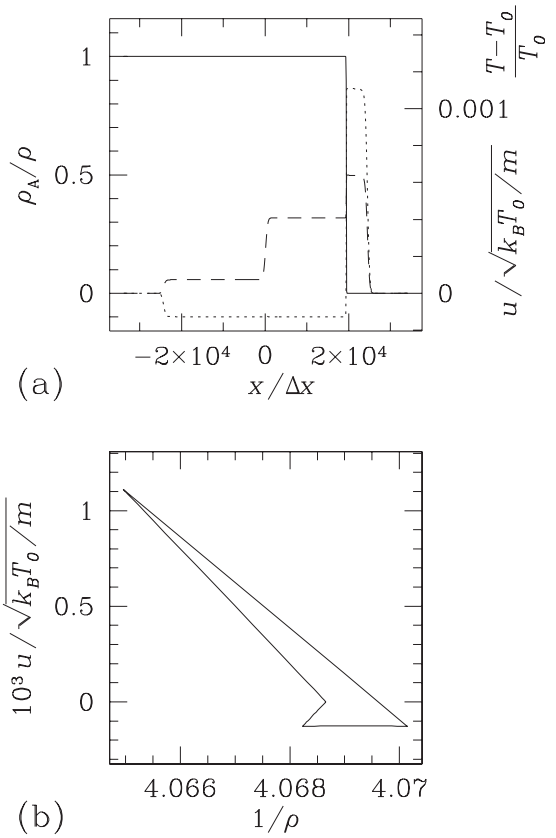

FIG. 4. Same caption as Fig. 3 for $E_a/k_BT_0=1.87$.

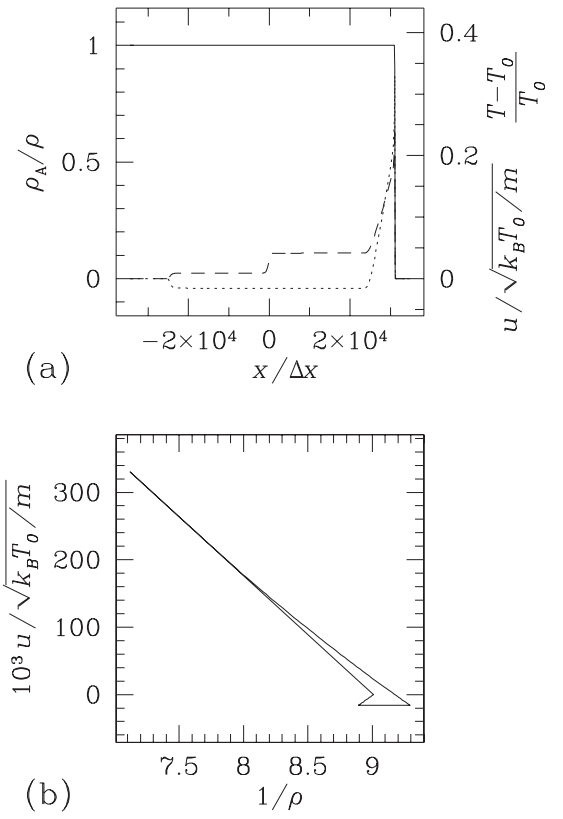

FIG. 5. Same caption as Fig. 3 for $E_a=1.34k_BT_0$ and $Q=k_BT_0$.

exothermic chemical wave front is controlled by the activation energy through the reaction rate and, to a lesser extent, by the heat release. For $Q>Q_c$, the chemical wave front becomes a Chapman-Jouguet detonation wave, whose speed is imposed by the heat release only. The critical value Q_c of the heat release associated with the bifurcation depends on the activation energy as shown in Fig. 2. In the case of a Chapman-Jouguet front replacing a supersonic, nondetonative chemical front, an analytical expression of the critical heat release can be computed. The bifurcation occurs for the value Q_c such that the upper branch U_{vdW+} reaches the unperturbed thermoneutral front speed, i.e., $U_{vdW+}(Q_c)=U(Q=0)$. In the case of a subsonic chemical front, the prediction of the critical heat release value is less obvious. The branch $U_{vdW-}(Q)$ given in Fig. 2 is an approximate result obtained by replacing the hydrodynamic variable values by the corresponding unperturbed values. The bifurcation is expected to occur when the F-KPP front speed $U(Q)$ reaches the lower branch $U_{vdW-}(Q)$. However, both $U(Q)$ and $U_{vdW-}(Q)$ depend on the ahead hydrodynamic variables which are perturbed by the shock wave.

The comparison with combustion is fruitful. As already mentioned, the initial conditions are different from usual ignition processes. From a mechanical point of view, we start from a homogeneous medium and the wave is only initiated by chemical species heterogeneity. On the contrary, combustion is generally ignited by a pressure or a temperature gradient. The so-called deflagration to detonation transition (DDT) [48–50] during which a (subsonic) deflagration wave becomes a (supersonic) detonation wave occurs in the course of time and should not be confused with the bifurcation observed here as heat release, viewed as a control parameter, is increased.

F. Differences between the perfect gas and van der Waals fluids

The perfect gas approximation for a van der Waals fluid can lead to qualitatively wrong predictions of the wave front dynamics. The forbidden domain limited by $U_{vdW\pm}$ spreads out around the straight line defined by the sound speed value $U_{S_{vdW}}$ at the unperturbed temperature and density. According to Eq. (25) and Fig. 1, the van der Waals sound speed strongly differs from the perfect gas sound speed $U_{S_{PG}}$.

For the van der Waals gas of density $\rho_0=0.163\rho_c$, at temperature $T_0=T_c$, the sound speed is smaller than $U_{S_{PG}}$. As observed in Fig. 2(a), this leads to the existence of a bounded domain in the (Q,U) diagram, under the lower branch U_{PG-} and above the upper branch U_{vdW+}, where the perfect gas approximation predicts *subsonic* diffusion flames, whereas a van der Waals gas leads to *supersonic* diffusion flames. Qualitatively, the application of the theory to the perfect gas leads to profiles of the type of Fig. 4 instead of those of Fig. 3. Moreover, the perfect gas approach precludes the observation of stationary chemical fronts in the forbidden domain limited by $U_{PG\pm}$, but steady supersonic diffusion flames are predicted for a van der Waals gas in the part of this domain which is above the upper branch U_{vdW+}.

For the dense, supercritical van der Waals fluid of density $\rho_0=1.23\rho_c$, at temperature $T_0=2T_c$, the sound speed is larger than $U_{S_{PG}}$. Figure 2(b) shows the existence of a bounded domain limited by the lower branch U_{vdW-} and the upper branch U_{PG+}. Now, the perfect gas approximation predicts *supersonic* diffusion flames whereas *subsonic* diffusion flames are expected in a dense, supercritical van der Waals fluid. Typically, profiles of the type of Fig. 3 should be obtained for a perfect gas when profiles of the type of Fig. 4 are observed for a dense, van der Waals supercritical fluid. In addition, supersonic diffusion flames are predicted for a perfect gas in the part of the forbidden domain associated with a dense, supercritical fluid, which is between $U_{vdW\pm}$ and above the upper branch U_{PG+}. Consequently, for activation energy and heat release values associated with this (Q,U) domain, the van der Waals approach predicts the observation of a Chapman-Jouguet detonation whereas it is a weak deflagration (subsonic diffusion flame) which is expected for a perfect gas. In this domain, the profiles look like those of Fig. 5 for a dense, supercritical van der Waals fluid whereas they would be of the type of Fig. 3 for a perfect gas. In addition, the propagation speed U_{vdW+} of the Chapman-Jouguet detonation wave in a dense, supercritical van der Waals fluid is much larger than the one predicted by the perfect gas approach.

V. CONCLUSIONS

We have presented an analytical and computational study of the steady dynamics of a traveling chemical wave front in a van der Waals fluid undergoing an exothermic, autocatalytic reaction of the Fisher-Kolmogorov-Petrovsky-Piskunov type. Contrary to usual combustion ignition processes, the initial nonuniformity of the reactive medium has been modeled by a step in species concentration. Similarly to what was done for a perfect gas in references [14,15], a forbidden interval of stationary wave front speeds has been shown to exist for nonideal fluids. A bifurcation between different combustion modes (between sub/supersonic diffusion flames and Chapman-Jouguet detonation waves) has likewise been revealed. Numerical results have been compared to analytical calculations so as to assess the modifications due to the van der Waals parameters, for low and high fluid densities. The shape of the forbidden domain is not sensitively deformed but it is shifted toward smaller wave front speeds at low densities and toward larger speeds at high densities. In particular, the speed of a Chapman-Jouguet detonation wave in a dense, van der Waals fluid is much higher than for a perfect gas. The bifurcation between a diffusion flame and a Chapman-Jouguet detonation wave reported here is not to be confused with the deflagration to detonation transition (DDT) [48–50]. The latter is observed in the course of time whereas the bifurcation occurs when the heat release is varied and reaches a critical value Q_c. However, DDT could be further investigated in the framework of our model, for an appropriate choice of the activation energy and heat release. We expect a non trivial relaxation toward the Chapman-Jouguet propagation speed for a sufficiently high activation energy and a heat release slightly larger than the critical value Q_c. In addition, it could be valuable to extend the macroscopic description presented here by a microscopic approach including the description of the fluctuations in the vicinity of the bifurcation.

This study focused on van der Waals fluids but can be readily extended to an equation of state describing other nonideal fluids, provided the transport coefficients are known. Even if it was restricted to the gaseous state of matter, the procedure of obtaining the forbidden interval is general and can be extended in both liquid and solid phases.

ACKNOWLEDGMENTS

This work was supported by the French-Polish joint project Partenariat Hubert Curien Polonium under Grant No. 20091NG. B.N. acknowledges support from Université Pierre et Marie Curie.

[1] A. G. Merzhanov and E. N. Rumanov, Rev. Mod. Phys. **71**, 1173 (1999).
[2] V. V. Bychkov and M. A. Liberman, Phys. Rep. **325**, 115 (2000).
[3] C. K. Law, *Combustion Physics* (Cambridge University Press, New York, 2006).
[4] I. Glassman and R. A. Yetter, *Combustion*, 4th ed. (Academic Press, New York, 2008).
[5] M. C. Cross and P. C. Hohenberg, Rev. Mod. Phys. **65**, 851 (1993).
[6] B. H. Gilding and R. Kersner, *Travelling Waves in Nonlinear Diffusion-Convection Reaction* (Birkhäuser, Basel, 2004).
[7] J. D. Murray, *Mathematical Biology: I. An Introduction* (Springer, New York, 2002).
[8] J. D'Hernoncourt, S. Kalliadasis, and A. De Wit, J. Chem. Phys. **123**, 234503 (2005).
[9] J. D'Hernoncourt, A. De Wit, and A. Zebib, J. Fluid Mech. **576**, 445 (2007).
[10] J. D'Hernoncourt, A. Zebib, and A. De Wit, Chaos **17**, 013109 (2007).
[11] P. Grosfils, F. Dubois, C. Yourassowsky, and A. De Wit, Phys. Rev. E **79**, 017301 (2009).
[12] J. S. Hansen, B. Nowakowski, and A. Lemarchand, J. Chem. Phys. **125**, 044313 (2006).
[13] B. Nowakowski and A. Lemarchand, J. Chem. Phys. **127**, 174712 (2007).
[14] M. Leda, A. Lemarchand, and B. Nowakowski, Phys. Rev. E **75**, 056304 (2007).
[15] G. Dumazer, M. Leda, B. Nowakowski, and A. Lemarchand, Phys. Rev. E **78**, 016309 (2008).
[16] F. A. Williams, *Combustion Theory*, 2nd ed. (Benjamin-Cummings, New York, 1985).
[17] J. W. Dold, Combust. Theory Modell. **11**, 909 (2007).
[18] R. A. Fisher, Ann. Eugen. **7**, 355 (1937).

[19] A. N. Kolmogorov, I. G. Petrovsky, and N. S. Piskunov, Bull. Univ. Moscow., Ser. Int. Sec. A **1**, 1 (1937).
[20] D. J. Needham, A. C. King, and J. H. Merkin, IMA J. Appl. Math. **53**, 137 (1994).
[21] B. Lucas, G. Gregoire, J. Lemaire, P. Maitre, J. M. Ortega, A. Rupenyam, B. Reimann, J. P. Schermann, and C. Desfrancois, Phys. Chem. Chem. Phys. **6**, 2659 (2004).
[22] M. Guisnet, P. Andy, N. S. Gnep, E. Benazzi, and C. Travers, Oil Gas Sci. Technol. **54**, 23 (1999).
[23] L. Domokos, L. Lefferts, K. Seshan, and J. A. Lercher, J. Catal. **197**, 68 (2001).
[24] M. Kangas, T. Salmi, and D. Y. Murzin, Ind. Eng. Chem. Res. **47**, 5413 (2008).
[25] L. D. Landau and E. M. Lifshitz, *Fluid Mechanics* (Pergamon Press, Oxford, 1987).
[26] A. M. Bartenev and B. E. Gelfand, Prog. Energy Combust. Sci. **26**, 29 (2000).
[27] J. H. Lee, R. Knystautas, and N. Yoshikawa, Acta Astronaut. **5**, 971 (1978).
[28] L. He and P. Clavin, Twenty-Fourth Symposium (International) on Combustion The Combustion Institute, Pittsburgh, 1992 (unpublished).
[29] N. N. Smirnov and I. I. Panfilov, Combust. Flame **101**, 91 (1995).
[30] R. Menikoff and B. J. Plohr, Rev. Mod. Phys. **61**, 75 (1989).
[31] B. M. Argrow, Shock Waves **6**, 241 (1996).
[32] P. Colonna and A. Guardone, Phys. Fluids **18**, 056101 (2006).
[33] D. Chandler, J. D. Weeks, and H. C. Andersen, Science **220**, 787 (1983).
[34] J. P. Hansen and I. R. McDonald, *Theory of Simple Liquids*, 3rd ed. (Academic Press, Amsterdam, 2006).
[35] M. S. Cramer and R. Sen, Phys. Fluids **30**, 377 (1987).
[36] M. S. Cramer, J. F. Monaco, and B. M. Fabeny, Phys. Fluids **6**, 674 (1994).
[37] H. J. Curran, M. P. Dunphy, J. M. Simmie, C. K. Westbrook, and W. J. Pitz, Proc. Combust. Inst. **24**, 769 (1992).
[38] W. K. Metcalfe, W. J. Pitz, H. J. Curran, J. M. Simmie, and C. K. Westbrook, Proc. Combust. Inst. **31**, 377 (2007).
[39] K. Yasunaga, Y. Kuraguchi, R. Ikeuchi, H. Masaoka, O. Takahashi, T. Koike, and Y. Hidaka, Proc. Combust. Inst. **32**, 453 (2009).
[40] F. Schlögl, Z. Phys. **253**, 147 (1972).
[41] Y. B. Zel'dovich and D. A. Frank-Kamenetskii, Dokl. Akad. Nauk SSSR **19**, 693 (1938).
[42] N. F. Carnahan and K. E. Starling, J. Chem. Phys. **51**, 635 (1969).
[43] Y. Song, E. A. Mason, and R. M. Stratt, J. Phys. Chem. **93**, 6916 (1989).
[44] M. Abramowitz and I. A. Stegun, *Handbook of Mathematical Functions with Formulas, Graphs and Mathematical Tables* (Dover, New York, 1964).
[45] P. Atkins and J. de Paula, *Atkins' Physical Chemistry* (Oxford University Press, Oxford, 2006).
[46] J. H. S. Lee, *The Detonation Phenomenon* (Cambridge University Press, New York, 2008).
[47] E. Brunet and B. Derrida, Phys. Rev. E **56**, 2597 (1997).
[48] A. K. Kapila, D. W. Schwendeman, J. J. Quirk, and T. Hawa, Combust. Theory Modell. **6**, 553 (2002).
[49] E. S. Oran and V. N. Gamezo, Combust. Flame **148**, 4 (2007).
[50] M. A. Liberman, M. Kuznetsov, A. Ivanov, and I. Metsukov, Phys. Lett. A **373**, 501 (2009).